

NORTHERN SKY GALACTIC COSMIC RAY ANISOTROPY BETWEEN 10 AND 1000 TEV WITH THE TIBET AIR SHOWER ARRAY

M. AMENOMORI¹, X. J. BI², D. CHEN³, T. L. CHEN⁴, W. Y. CHEN², S. W. CUI⁵, DANZENGLUOBU⁴, L. K. DING², C. F. FENG⁶, ZHAOYANG FENG², Z. Y. FENG⁷, Q. B. GOU², Y. Q. GUO², H. H. HE², Z. T. HE⁵, K. HIBINO⁸, N. HOTTA⁹, HAIBING HU⁴, H. B. HU², J. HUANG², H. Y. JIA⁷, L. JIANG², F. KAJINO¹⁰, K. KASAHARA¹¹, Y. KATAYOSE¹², C. KATO¹³, K. KAWATA¹⁴, M. KOZAI^{13,a}, LABACIREN⁴, G. M. LE¹⁵, A. F. LI^{16,6,2}, H. J. LI⁴, W. J. LI^{2,7}, C. LIU², J. S. LIU², M. Y. LIU⁴, H. LU², X. R. MENG⁴, T. MIYAZAKI¹³, K. MIZUTANI^{11,17}, K. MUNAKATA¹³, T. NAKAJIMA¹³, Y. NAKAMURA¹³, H. NANJO¹, M. NISHIZAWA¹⁸, T. NIWA¹³, M. OHNISHI¹⁴, I. OHTA¹⁹, S. OZAWA¹¹, X. L. QIAN^{6,2}, X. B. QU², T. SAITO²⁰, T. Y. SAITO²¹, M. SAKATA¹⁰, T. K. SAKO¹⁴, J. SHAO^{2,6}, M. SHIBATA¹², A. SHIOMI²², T. SHIRAI⁸, H. SUGIMOTO²³, M. TAKITA¹⁴, Y. H. TAN², N. TATEYAMA⁸, S. TORII¹¹, H. TSUCHIYA²⁴, S. UDO⁸, H. WANG², H. R. WU², L. XUE⁶, Y. YAMAMOTO¹⁰, K. YAMAUCHI¹², Z. YANG², A. F. YUAN⁴, T. YUDA^{14,b}, L. M. ZHAI³, H. M. ZHANG², J. L. ZHANG², X. Y. ZHANG⁶, Y. ZHANG², YI ZHANG², YING ZHANG², ZHAXISANGZHU⁴, X. X. ZHOU⁷
(THE TIBET AS γ COLLABORATION)

¹Department of Physics, Hirosaki University, Hirosaki 036-8561, Japan

²Key Laboratory of Particle Astrophysics, Institute of High Energy Physics, Chinese Academy of Sciences, Beijing 100049, China

³National Astronomical Observatories, Chinese Academy of Sciences, Beijing 100012, China

⁴Department of Mathematics and Physics, Tibet University, Lhasa 850000, China

⁵Department of Physics, Hebei Normal University, Shijiazhuang 050016, China

⁶Department of Physics, Shandong University, Jinan 250100, China

⁷Institute of Modern Physics, Southwest Jiaotong University, Chengdu 610031, China

⁸Faculty of Engineering, Kanagawa University, Yokohama 221-8686, Japan

⁹Faculty of Education, Utsunomiya University, Utsunomiya 321-8505, Japan

¹⁰Department of Physics, Konan University, Kobe 658-8501, Japan

¹¹Research Institute for Science and Engineering, Waseda University, Tokyo 169-8555, Japan

¹²Faculty of Engineering, Yokohama National University, Yokohama 240-8501, Japan

¹³Department of Physics, Shinshu University, Matsumoto 390-8621, Japan

¹⁴Institute for Cosmic Ray Research, University of Tokyo, Kashiwa 277-8582, Japan

¹⁵National Center for Space Weather, China Meteorological Administration, Beijing 100081, China

¹⁶School of Information Science and Engineering, Shandong Agriculture University, Taian 271018, China

¹⁷Saitama University, Saitama 338-8570, Japan

¹⁸National Institute of Informatics, Tokyo 101-8430, Japan

¹⁹Sakushin Gakuin University, Utsunomiya 321-3295, Japan

²⁰Tokyo Metropolitan College of Industrial Technology, Tokyo 116-8523, Japan

²¹Max-Planck-Institut für Physik, München D-80805, Deutschland

²²College of Industrial Technology, Nihon University, Narashino 275-8576, Japan

²³Shonan Institute of Technology, Fujisawa 251-8511, Japan

²⁴Japan Atomic Energy Agency, Tokai-mura 319-1195, Japan

^a now at: ISAS/JAXA Sagamihara 252-5210, Japan

^b Deceased.

Draft version March 3, 2017

ABSTRACT

We report on the analysis of the 10–1000 TeV large-scale sidereal anisotropy of Galactic cosmic rays (GCRs) with the data collected by the Tibet Air Shower Array from 1995 October to 2010 February. In this analysis, we improve the energy estimate and extend the decl. range down to -30° . We find that the anisotropy maps above 100 TeV are distinct from that at a multi-TeV band. The so-called tail-in and loss-cone features identified at low energies get less significant, and a new component appears at ~ 100 TeV. The spatial distribution of the GCR intensity with an excess (7.2σ pre-trial, 5.2σ post-trial) and a deficit (-5.8σ pre-trial) are observed in the 300 TeV anisotropy map, in close agreement with IceCube’s results at 400 TeV. Combining the Tibet results in the northern sky with IceCube’s results in the southern sky, we establish a full-sky picture of the anisotropy in hundreds of TeV band. We further find that the amplitude of the first order anisotropy increases sharply above ~ 100 TeV, indicating a new component of the anisotropy. All these results may shed new light on understanding the origin and propagation of GCRs.

1. INTRODUCTION

The arrival directions of Galactic cosmic rays (GCRs) are nearly isotropic due to deflections in the Galactic magnetic field (GMF). Only weak anisotropy is expected from the diffusion and/or drift of GCRs in GMF. Observations of ground-based air shower arrays and underground muon detectors do show the existence of small anisotropies with relative amplitudes of the order of 10^{-4}

to 10^{-3} at energies from 100 GeV to hundreds of TeV (see Figure 5). However, the variation of the amplitude with energy seems to be difficult to interpret in terms of the conventional GCR diffusion model in the Galaxy (*e.g.* (Moskalenko et al. 2002; Ahlers & Mertsch 2016)). The study of GCR anisotropy, therefore, is important to understand the origin and propagation of GCRs.

Only a few results of the anisotropy in the energy range from hundreds of TeV up to ~ 10 PeV have been re-

ported, primarily due to the low fluxes of cosmic rays (CRs) in this energy range. EAS-TOP collaboration reported for the first time a detection of anisotropy at ~ 200 TeV (Aglietta et al. 1996). With the accumulation of data, they improved their result later and reported a sharp increase of the anisotropy amplitude at primary energies around ~ 370 TeV (Aglietta et al. 2009). At the PeV energy region, the Akeno experiment reported an increase of the CR anisotropy amplitude in 1986 (Kifune et al. 1986). No hint of the anisotropy, on the other hand, has been found in the KASCADE data at higher energies between 0.7 and 6 PeV (Antoni et al. 2004). Recently, the IceCube collaboration reported the anisotropy observed in the southern sky, showing a new feature different from that obtained by EAS-TOP (Abbasi et al. 2012). A clear deficit with a post-trial significance of -6.3σ at 400 TeV was detected, which was then confirmed by the result from Ice-Top (Aartsen et al. 2013). The Ice-Top data further revealed the existence of anisotropy at energies up to 1 PeV (Aartsen et al. 2013).

The Tibet Air Shower (AS) array collaboration presented the first two-dimensional anisotropy measurements in an energy region from several TeV to several hundred TeV. The anisotropy features, known as the “tail-in” and “loss-cone” features, were observed with very high significances (Amenomori et al. 2006). A new component anisotropy at multi-TeV energies from the Cygnus direction was also reported (Amenomori et al. 2006). It has been shown that the amplitude of the first order anisotropy decreases above a few hundred TeV, indicating the co-rotation of GCRs around the Galactic center. With more data accumulated, hints of ~ 300 TeV anisotropies have been revealed (Feng et al. 2009; Amenomori et al. 2013). The anisotropy feature was found to be different from those in lower energy regions and in agreement with IceCube’s result at 400 TeV (Abbasi et al. 2012). These analyses of Tibet AS array data cover decl. from -15° to 75° , yet leaving a gap to be connected with IceCube’s result in the southern sky. Here we extend these analyses to include events with zenith angle up to 60° , which corresponds to a coverage of decl. from -30° to 90° (Amenomori et al. 2015). Combining with IceCube’s results, we present for the first time a full-sky anisotropy observed at hundreds of TeV. By improving the reconstruction of primary energy, we will also extend the analyzed energy range to two decades between 10 TeV and 1 PeV, which is also the widest coverage of such works.

2. ANALYSIS

2.1. Experiment and Data reconstruction

The Tibet AS Array is located at Yangbajing in Tibet, China (90.522°E , 30.102°N , 4300 m above sea level, 606 g/cm² atmospheric depth). The detector array consists of plastic scintillation detectors with an area of 0.5 m² each. The effective area of the Tibet AS array has been gradually enlarged, via adding the same-type detectors to the array. The Tibet I array was constructed in 1990, using 65 plastic scintillation detectors placed on grids with 15 m spacing. It was then upgraded to 221 detectors on 15 m grids, covering a total of $36,900$ m², known as the Tibet II array. It began operation in 1995 October, with a trigger rate of ~ 230 Hz. The Tibet II was then

upgraded to the current Tibet III, a denser array with 7.5 m grids, in 1999 and 2003 (Amenomori et al. 2003). The trigger rate is ~ 1700 Hz for the Tibet III array.

In order to maintain the uniformity of the array performance, we analyze the data keeping the same configuration of the Tibet II array throughout the observation period from 1995 October to 2010 February, so that the full data sample taken by Tibet II and Tibet III array can be used in the present analysis. The traditional shower reconstruction procedure is applied to get all the parameters of one shower, such as the core position, zenith, and azimuth angles (θ , ϕ) of the incident direction and shower size $\sum \rho_{FT}$ (the sum of the number of particles per m² counted by all the fast-timing [FT] detector). The following three criteria are applied to select events for further analyses: (1) each AS event should fire four or more detectors, with each recording 1.25 or more particles; (2) the AS core position should be located inside the array; and (3) zenith angle $\theta < 60^\circ$.

2.2. Estimation of the CR Energy

The ASs reaching the array with a large zenith angle θ travel through a larger slant atmospheric depth than the vertical ones. This leads to a zenith angle dependence of the relation between $\sum \rho_{FT}$ and the primary particle energy. In most of the previous works of the Tibet AS γ Collaboration (Amenomori et al. 2003, 2005a, 2006; Feng et al. 2009; Amenomori et al. 2013), the shower size $\sum \rho_{FT}$ is solely adopted to infer the primary energy of an AS without considering the zenith angle dependence. This approximation works well for small zenith angles ($\theta < \sim 40^\circ$), considering the natural fluctuation in the development of the AS and the limited resolution of the primary energy.

In this work, we intend to explore the anisotropy with decl. down to -30° by including showers with zenith angles up to 60° . Therefore, the zenith angle dependence of the energy reconstruction must be taken into account. We develop a two-dimensional selection criterion in the $\sum \rho_{FT} - \sec\theta$ plane for the energy reconstruction.

The uncertainty of the CR energy reconstruction has been estimated with a full Monte Carlo (MC) simulation of CR interactions in the atmosphere by CORSIKA (version 6.204; (Heck et al. 1998). The hadronic interaction model QGSJET01c and the detector response modeled by Epics (version 8.65; (Kasahara 2006) are used. In this simulation, we adopt the composition and spectrum models of primary CRs given in (Hörandel 2003) as inputs.

Figure 1 shows the simulated distribution in the primary CR energy as a function of $\sum \rho_{FT}$ and $\sec\theta$. It shows that for a given range of $\sum \rho_{FT}$, small zenith angle events (at $\sec\theta \sim 1$) are dominated by CRs with lower average energy, compared with large zenith angle events (at $\sec\theta \sim 2$). We show regions of constant primary energies (15, 50, 100, 300, and 1000 TeV) in the plane of ($\sum \rho_{FT}$, $\sec\theta$) as regions delimited by the dashed lines in Figure 1. This grouping enables us to select events in five energy samples with minimal overlappings.

Figure 2 shows the simulated primary energy distributions of the five energy samples, as indicated by the dashed lines in Figure 1. The uncertainty of the primary energy estimate is dominated by the fluctuation of the AS. Event numbers in five energy samples are 2.33×10^{10}

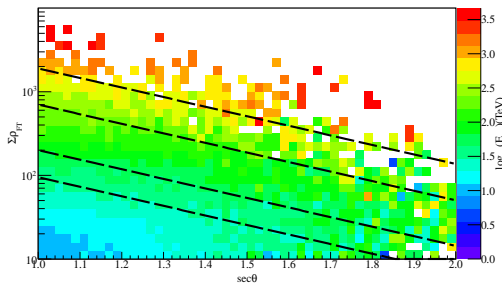


FIG. 1.— Simulated distribution of the log-mean energy of primary CRs as a function of $\sum \rho_{FT}$ and zenith angle. The y -axis is $\sum \rho_{FT}$; the x -axis is $\sec \theta$, where θ is the reconstructed zenith angle; and the color scale represents the reconstructed log-mean energy in units of TeV. Dashed lines mark out the borders of events with different energies (15, 50, 100, 300, and 1000 TeV).

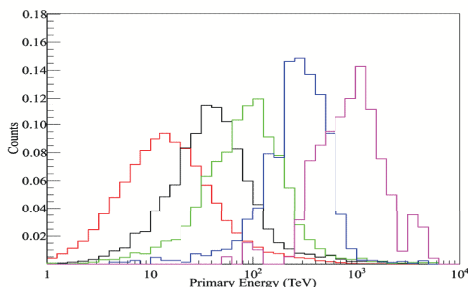


FIG. 2.— Normalized event number as a function of the simulated primary energy in each of the five energy samples, based on MC data. The log-mean energies of the five samples are 15 TeV (red), 50 TeV (black), 100 TeV (green), 300 TeV (blue), and 1 PeV (pink).

(15 TeV), 3.97×10^9 (50 TeV), 1.96×10^9 (100 TeV), 2.71×10^8 (300 TeV), and 5.72×10^7 (1 PeV), as listed in Table 1.

2.3. Analysis of the first harmonics of the anisotropy

We employ the All-Distance Equi-Zenith Angle Method (Amenomori et al. 2005a, 2006), which has been shown to be sensitive to probe the large-scale anisotropy, to analyze the data. Details about this method can be found in (Amenomori et al. 2005a). The sky of the horizontal coordinate is divided into cells with a bin size of 1° in both zenith (from 0° to 60°) and azimuth (from 0° to 360°). For the equatorial coordinate, the sky is divided into cells of $2^\circ \times 2^\circ$ between 0° and 360° in the R.A. (α) and between -30° and 90° in the decl. (δ). The two-dimensional (2D) map in the equatorial coordinate is then smoothed in a window, changing the window widths between 5 and 30° .

To quantify the magnitude of the anisotropy, we project the two-dimensional (2D) anisotropy map before smoothing onto the R.A. axis, through averaging the relative intensities in all declinations from -30° to 90° , to derive the one-dimensional (1D) profile of the anisotropy. The R.A. is binned into 18 bins for this 1D analysis, and the 1D profile of the anisotropy is fitted by the first order harmonic function in form of

$$R(\alpha) = 1 + A_1 \cos(\alpha - \phi_1), \quad (1)$$

where $R(\alpha)$ denotes the relative intensity of CRs at R.A. α , A_1 is the amplitude of the first harmonics, and ϕ_1 is the phase at which $R(\alpha)$ reaches its maximum.

3. RESULTS

3.1. Sidereal Anisotropy map at 300 TeV

Figure 3 shows the significance map and the relative intensity map of the sidereal anisotropy for the 300 TeV energy sample. A smoothing with an optimized window width of 30° is applied in this figure. We combined the 300 TeV and 1 PeV samples together in this figure to increase the statistics. The total event number used in this figure is 3.28×10^8 , and the median energy is approximately 300 TeV.

From the significance map, we find that two regions are significant—that is, an excess centered at ($\alpha = 263^\circ$, $\delta = 11^\circ$) with a significance of 7.2σ and a deficit centered at ($\alpha = 93^\circ$, $\delta = -25^\circ$) with a significance of -5.8σ . Note that the significance values are the pre-trial results. We conservatively estimate a trial factor by assuming that all scans give statistically independent results. Since the search for this excess is performed over about 60×180 cells, and 26 different smoothing radii, the total trial factor is estimated to be about 2.81×10^5 . The post-trial significance of the excess is $\sim 5.2\sigma$. The deficit is no longer significant, fail to reach the 5σ level, after the correction for the trials.

Because the acceptance of the detector decreases for larger zenith angles, the relative intensity map is similar but not completely the same as the significance map. An excess region centered at ($\alpha = 269^\circ$, $\delta = -13^\circ$) with a maximum excess of $+1.38 \times 10^{-3}$, and a deficit region centered at ($\alpha = 87^\circ$, $\delta = -29^\circ$) with a maximum deficit of -1.80×10^{-3} can be seen. Both the excess and deficit regions are consistent with the results of IceCube at 400 TeV in the southern hemisphere (Abbasi et al. 2012). Combining these results gives us a full-sky picture of the sidereal anisotropy of GCRs at hundreds of TeV.

The bottom panel in Figure 3 also shows the 1D projection of the relative intensity before the smoothing onto the R.A. axis. The correlation among different bins is carefully considered when calculating the statistical errors and fitting the data with the harmonic function in equation 1. If the correlation is not considered correctly, the errors of the fitting parameters would be underestimated. The blue curve shows the best-fitting result, with the fitting parameters indicated in the figure. The significance of non-zero amplitude is 5.6σ , which shows that the obtained first harmonics are indeed significant. The reduced χ^2 value is 26.7/16, which means that the first harmonic function can describe the 1D projected profile well.

One of the possible origins of the sidereal anisotropy is the Compton-Getting (CG) effect, due to the orbital motion of the solar system around the Galactic center (Compton & Getting 1935). The relative intensity of this effect is carefully calculated by the MC method. Considering the location of the Tibet AS array (90.522°E , 30.102°N), the velocity (220 km s^{-1}) of the orbital motion of the solar system around the Galactic center and the spectrum index (2.7) of the CRs energy spectrum, the intensity of the sky that is divided into cells of $2^\circ \times 2^\circ$ between 0° and 360° in the R.A. (α) and between -30° and 90° in the decl. (δ) is calculated. Then the identical analyses are performed to this MC data sample.

The $R(\alpha)$ expected from this CG effect, shown as the black dashed line in Figure 3, has a maximum at ($\alpha = 315^\circ$, $\delta = 0^\circ$) and a minimum at ($\alpha = 135^\circ$, $\delta = 0^\circ$). Neither the amplitude nor the phase of the large-scale anisotropy observed in this work can be described in terms of the CG effect.

3.2. Variation of CR sidereal anisotropy with the energy between 10 and 1000 TeV

Figure 4 shows the variation of the sidereal anisotropy with the energy between 10 TeV and 1 PeV. At 15 TeV and 50 TeV, the tail-in and loss-cone features (Amenomori et al. 2006) are observed with very high significances. An intensity excess in the Cygnus region can also be seen. However, these features become less significant above 100 TeV, being replaced with some new features. At 300 TeV and 1 PeV, the anisotropy maps are distinctly different from those in 15-50 TeV. We can clearly see the phase of the 1D projection changing with the primary energies, as seen in Table 1, showing the best-fit parameters.

Figure 5 compares the amplitude and phase obtained in this work with those reported so far from the deep underground muon experiments and extensive AS experiments. Our results are in close agreement with other results in similar energy regions in both the amplitude and the phase. It is interesting to note that a sharp increase of the amplitude above 100 TeV can be seen in the upper panel. The origins of this feature cannot be explained with the conventional diffusion scenario of GCRs, and may provide us with a new hint for understanding the origin and propagation of GCRs.

3.3. Anisotropy in Solar Time and Antisidereal Time

In order to confirm that the obtained anisotropy is not affected by the seasonal variation of the AS array performance, identical analyses are performed in the solar time and antisidereal time frames in five energy samples. Figure 6 shows the local solar time and antisidereal time daily variations measured by Tibet AS Array in five energy samples, and the best-fit parameters are also shown in Table 1. The amplitude and phase in the solar time frame are in good agreement with the expectation from the CG effect due to the terrestrial orbital motion around the Sun ($A_{\text{sol,CG}} = 0.047\%$ and $\phi_{\text{sol,CG}} = 6.0$ hr). In all five energy samples, no significant anisotropy is observed in the antisidereal time frame, ensuring that no additional correction is required for the seasonal effects. The observed results in the solar and antisidereal time frames support the reliability of the observed sidereal anisotropy.

4. CONCLUSION AND DISCUSSION

Fifteen years data recorded by the Tibet AS array have been analyzed to study the sidereal anisotropy of CRs. In this work, we improve the estimate of the primary CR energies through a 2D cut in the $\sum \rho_{FT} - \sec\theta$ plane, to explore the anisotropy including larger zenith angle events. For the first time, we extend the analyzed decl. down to

-30° to complete a full-sky coverage of the anisotropy at hundreds of TeV energies by combining with the IceCube's results at the South Pole. The 2D anisotropy map at ~ 300 TeV obtained in this work is smoothly connected with IceCube's results at 400 TeV. The energy dependence of the large-scale sidereal anisotropy has been derived between 10 TeV and 1 PeV. We measured the energy dependence of the first harmonics of the anisotropy above 100 TeV, which may be associated with local origins of GCRs.

The CG effect expected from the orbital motion of the solar system around the Galactic center is not observed at 300 TeV, as shown in Figure 3. The basic picture that GCRs are co-rotating with the local Galactic neighbors still holds at this energy (Amenomori et al. 2006). As pointed out earlier, the GCR rest frame may have a smaller relative velocity with a different direction from neighboring stars and the interstellar medium (Abbasi et al. 2012). This scenario is possibly responsible for the GCR anisotropy observed at hundreds of TeV.

The strongest excesses at hundreds of TeV are from the direction of the Galactic center, which may imply a Galactic center origin of GCRs at these energies (Guo et al. 2013). It is interesting to note that the highest-energy CR accelerators have been identified by the HESS telescope in the Galactic center (HESS Collaboration et al. 2016). However, the energy dependences of the amplitude and phase cannot be easily understood in a simple diffusion scenario with any types of GCR sources.

The sharp increase of the amplitude above 100 TeV may imply an evolution of propagation parameters, such as spatial parameters (Tomassetti 2015; Guo et al. 2016). The knowledge of the propagation of GCRs needs to be further improved for our full understanding the properties of the anisotropy, especially in this high-energy region where the conventional diffusion/drift models may not work any more. Finally, we add to note that the measurements of the anisotropy above PeV, which is possibly associated with the knee of GCRs, are very important to advance our understanding of origin and propagation of GCRs.

5. ACKNOWLEDGMENTS

The collaborative experiment of the Tibet Air Shower Arrays has been performed under the auspices of the Ministry of Science and Technology of China and the Ministry of Foreign Affairs of Japan. This work was supported in part by a Grant-in-Aid for Scientific Research on Priority Areas from the Ministry of Education, Culture, Sports, Science and Technology, by Grants-in-Aid for Science Research from the Japan Society for the Promotion of Science in Japan, and by the Grants from the National Natural Science Foundation of China and the Chinese Academy of Sciences. Zhaoyang Feng is supported by the Natural Sciences Foundation of China (Nos.11405182, Nos.1135010). C. Liu is supported by the Natural Sciences Foundation of China (Nos. 11405180).

REFERENCES

Aartsen, M. G., Abbasi, R., Abdou, Y., et al. 2013, ApJ, 765, 55
Abbasi, R., Abdou, Y., Abu-Zayyad, T., et al. 2010, ApJ, 718, L194

—, 2012, ApJ, 746, 33
Abdo, A. A., Allen, B. T., Aune, T., et al. 2009, ApJ, 698, 2121

- Aglietta, M., Alessandro, B., Antonioli, P., et al. 1995, International Cosmic Ray Conference, 2, 800
— 1996, ApJ, 470, 501
- Aglietta, M., Alekseenko, V. V., Alessandro, B., et al. 2009, ApJ, 692, L130
- Ahlers, M., & Mertsch, P. 2016, ArXiv e-prints, arXiv:1612.01873
- Alekseenko, V. V., Cherniaev, A. B., Djappuev, D. D., et al. 2009, Nuclear Physics B Proceedings Supplements, 196, 179
- Alexeyenko, V. V., Chudakov, A. E., Gulieva, E. N., & Sbornichikov, V. G. 1981, International Cosmic Ray Conference, 2, 146
- Ambrosio, M., Antolini, R., Baldini, A., et al. 2003, Phys. Rev. D, 67, 042002
- Amenomori, M., Ayabe, S., Cui, S. W., et al. 2003, ApJ, 598, 242
- Amenomori, M., Ayabe, S., Chen, D., et al. 2005a, ApJ, 633, 1005
- Amenomori, M., Ayabe, S., Cui, S. W., et al. 2005b, ApJ, 626, L29
- Amenomori, M., Ayabe, S., Bi, X. J., et al. 2006, Science, 314, 439
- Amenomori, M., Bi, X. J., Chen, D., et al. 2013, Proceedings of the 33rd ICRC, Rio de Janeiro, ID256
— 2015, Proceedings of the 34th ICRC, the Haag, ID355
- Andreyev, Y. M., Chudakov, A. E., Kozyarivsky, V. A., et al. 1987, International Cosmic Ray Conference, 2, 22
- Antoni, T., Apel, W. D., Badea, A. F., et al. 2004, ApJ, 604, 687
- Bartoli, B., Bernardini, P., Bi, X. J., et al. 2015, ApJ, 809, 90
- Bercovitch, M., & Agrawal, S. P. 1981, International Cosmic Ray Conference, 10, 246
- Compton, A. H., & Getting, I. A. 1935, Physical Review, 47, 817
- Cutler, D. J., & Groom, D. E. 1991, ApJ, 376, 322
- Feng, Z., Zhang, Y., Liu, C., et al. 2009, Proceedings of the 31st ICRC, Łódź, ID0869
- Fenton, K. B., Fenton, A. G., & Humble, J. E. 1995, International Cosmic Ray Conference, 4, 635
- Gombosi, T., Kóta, J., Somogyi, A. J., et al. 1975, International Cosmic Ray Conference, 2, 586
- Guillian, G., Hosaka, J., Ishihara, K., et al. 2007, Phys. Rev. D, 75, 062003
- Guo, Y.-Q., Feng, Z.-Y., Yuan, Q., Liu, C., & Hu, H.-B. 2013, New Journal of Physics, 15, 013053
- Guo, Y.-Q., Tian, Z., & Jin, C. 2016, ApJ, 819, 54
- Heck, D., Knapp, J., Capdevielle, J. N., Schatz, G., & Thouw, T. 1998, CORSIKA: a Monte Carlo code to simulate extensive air showers.
- HESS Collaboration, Abramowski, A., Aharonian, F., et al. 2016, Nature, 531, 476
- Hörandel, J. R. 2003, Astroparticle Physics, 19, 193
- Kasahara, K. 2006, <http://cosmos.n.kanagawa-u.ac.jp/EPICSHome/index.html>
- Kifune, T., Hara, T., Hatano, Y., et al. 1986, Journal of Physics G Nuclear Physics, 12, 129
- Lee, Y. W., & Ng, L. K. 1987, International Cosmic Ray Conference, 2, 18
- Mori, S., Yasue, S., Munakata, K., et al. 1995, International Cosmic Ray Conference, 4, 648
- Moskalenko, I. V., Strong, A. W., Ormes, J. F., & Potgieter, M. S. 2002, ApJ, 565, 280
- Munakata, K., Yasue, S., Mori, S., et al. 1995, International Cosmic Ray Conference, 4, 639
- Munakata, K., Kiuchi, T., Yasue, S., et al. 1997, Phys. Rev. D, 56, 23
- Nagashima, K., Fujimoto, K., Sakakibara, S., Fujii, Z., & Ueno, H. 1989, Nuovo Cimento C Geophysics Space Physics C, 12, 695
- Sakakibara, S., Ueno, H., Fujimoto, K., Kondo, I., & Nagashima, K. 1973, International Cosmic Ray Conference, 2, 1058
- Swinson, D. B., & Nagashima, K. 1985, Planet. Space Sci., 33, 1069
- Thambyahpillai, T. 1983, International Cosmic Ray Conference, 3, 383
- Tomassetti, N. 2015, Phys. Rev. D, 92, 081301
- Ueno, H., Fujii, Z., & Yamada, T. 1990, International Cosmic Ray Conference, 6, 361

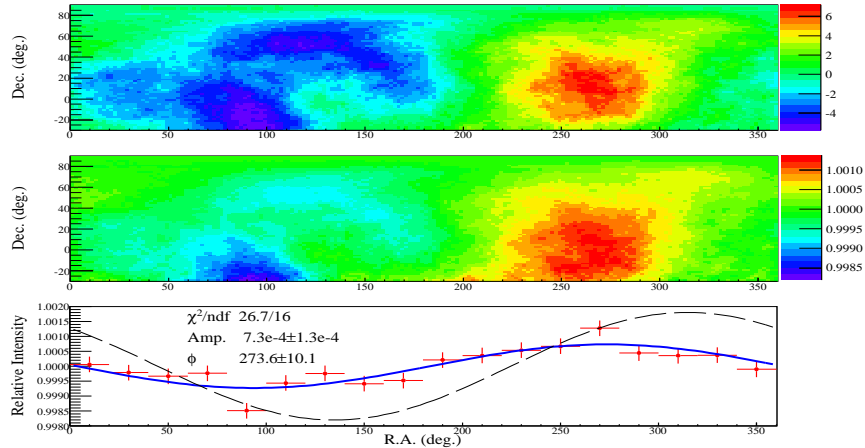


FIG. 3.— Large-scale sidereal anisotropy at 300 TeV by the Tibet AS Array. The 2D maps are smoothed with a 30° Gaussian kernel. The top and middle panels display the significance and relative intensity maps, respectively, while the bottom one shows the 1D projection of the 2D map onto the R.A. axis. The blue curve shows the first harmonic fitting to the data, and the black dashed line is the predicted Galactic CG effect with an amplitude of $\sim 0.19\%$.

TABLE 1

FITTING RESULTS OF THE FIRST HARMONIC (AMPLITUDE, PHASE, AND REDUCED χ^2) IN THE SIDEREAL (COLUMNS 2-4), SOLAR (COLUMNS 5-7), AND ANTISIDEREAL (COLUMNS 8-10) TIMES. THE NUMBER OF EVENTS IN EACH ENERGY SAMPLE IS GIVEN IN COLUMN 11.

Energy TeV	A_{sid} 10^{-4}	ϕ_{sid} [$^\circ$]	χ^2_{sid}/ndf	A_{sol} 10^{-4}	ϕ_{sol} hr	χ^2_{sol}/ndf	A_{asid} 10^{-4}	ϕ_{asid} hr	χ^2_{asid}/ndf	Number of Event
15	8.5 ± 0.2	21.9 ± 1.6	911./16	4.1 ± 0.2	6.05 ± 0.22	69.7/16.	0.53 ± 0.24	22.2 ± 1.7	24.4/16	2.33×10^{10}
50	5.3 ± 0.4	20.8 ± 4.7	152.9/16	4.6 ± 0.4	6.37 ± 0.35	46.7/16	0.39 ± 0.43	22.5 ± 4.2	46.7/16	3.97×10^9
100	2.7 ± 0.6	326.8 ± 12.0	67.6/16	4.0 ± 0.6	5.91 ± 0.53	14.2/16.	0.80 ± 0.56	22.3 ± 2.7	9.8/16	1.96×10^9
300	6.0 ± 1.4	267.1 ± 13.5	27.0/16.	3.5 ± 1.4	6.53 ± 1.56	19.0/16.	1.7 ± 1.4	5.3 ± 3.2	11.6/16	2.71×10^8
1000	13.0 ± 3.0	286.6 ± 12.6	9.3/16	9.8 ± 2.8	6.97 ± 1.13	10.9/16.	1.0 ± 2.9	14.8 ± 11.0	6.3/16	5.72×10^7

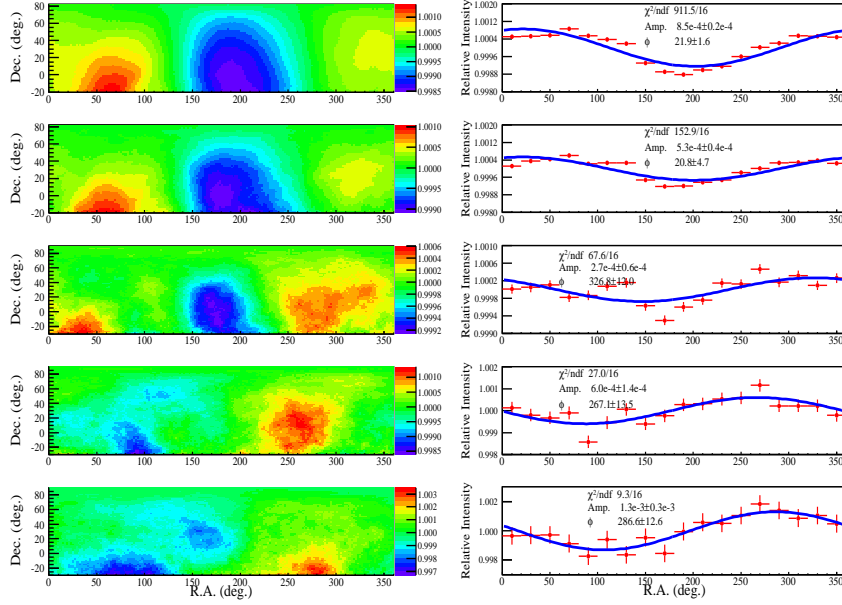


FIG. 4.— 2D anisotropy maps in five energy samples (15, 50, 100, 300, and 1000 TeV, from top to bottom). Left panels show the relative intensity maps (with 30° smoothing), while right panels show the 1D projections. The meaning of the blue curves in the right panels is the same as in Figure 3.

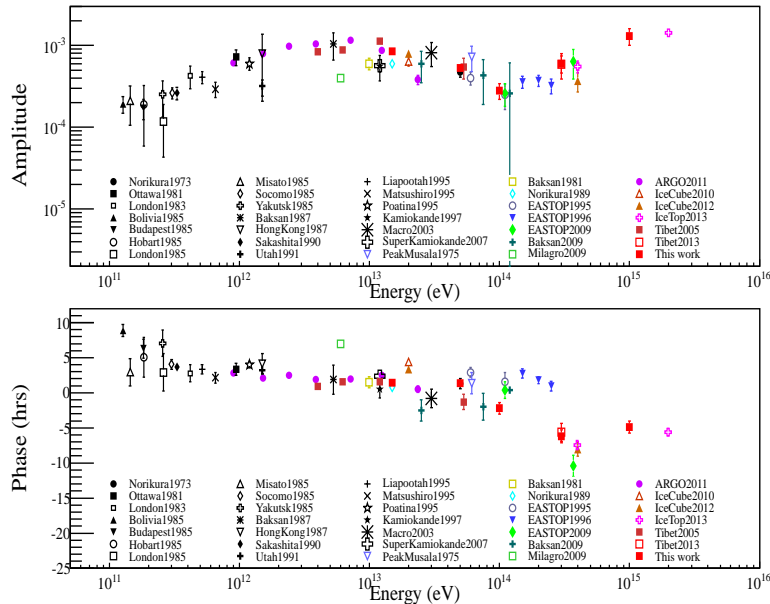


FIG. 5.— The energy dependences of amplitude (top) and phase (bottom) of the first harmonics of the CRs anisotropy obtained in this work, and reported from previous measurements. They are underground muon observations: Norikura(1973) (Sakakibara et al. 1973), Ottawa(1983) (Bercovitch & Agrawal 1981), London(1983) (Thambyahpillai 1983), Bolivia(1985) (Swinson & Nagashima 1985), Budapest(1985) (Swinson & Nagashima 1985), Hobart(1985) (Swinson & Nagashima 1985), London(1985) (Swinson & Nagashima 1985), Misato(1985) (Swinson & Nagashima 1985), Socorro(1985) (Swinson & Nagashima 1985), Yakutsk(1985) (Swinson & Nagashima 1985), Banksan(1987) (Andreyev et al. 1987), HongKong(1987) (Lee & Ng 1987), Sakashita(1990) (Ueno et al. 1990), Utah(1991) (Cutler & Groom 1991), Liapootah(1995) (Munakata et al. 1995), Matsushiro(1995) (Mori et al. 1995), Poatina(1995) (Fenton et al. 1995), Kamiokande(1997) (Munakata et al. 1997), Marco(2003) (Ambrosio et al. 2003), SuperKamiokande(2007) (Guillian et al. 2007), and air shower array experiments: PeakMusala(1975) (Gombosi et al. 1975), Baksan(1981) (Alexeyenko et al. 1981), Norikura(1989) (Nagashima et al. 1989), EASTOP(1995,1996,2009) (Aglietta et al. 1995, 1996, 2009), Baksan(2009) (Alekseenko et al. 2009), Milagro(2009) (Abdo et al. 2009), IceCube(2010,2012) (Abbasi et al. 2010, 2012), IceTop(2013) (Aartsen et al. 2013), ARGO-YBJ(2015) (Bartoli et al. 2015), Tibet(2005,2013) (Amenomori et al. 2005b; Amenomori et al. 2013).

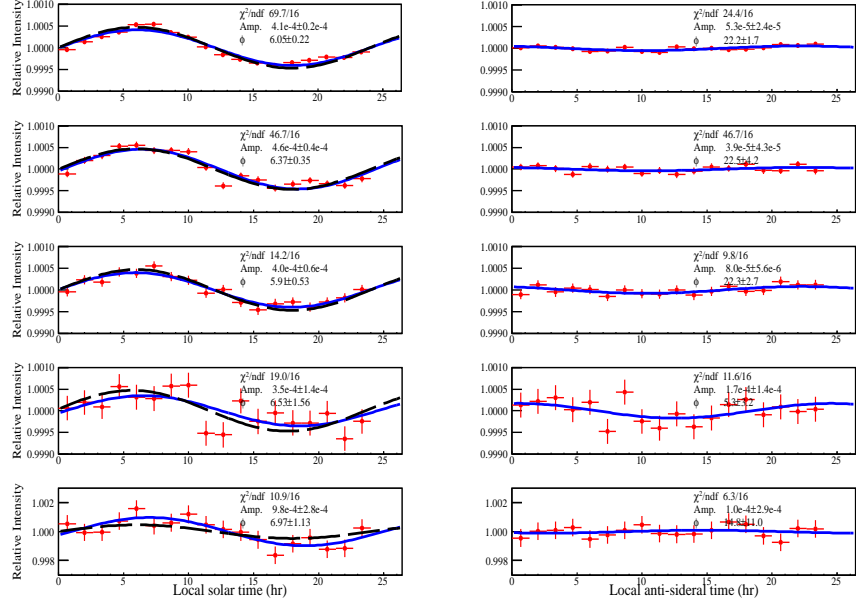


FIG. 6.— Local solar time and antisidereal time daily variations measured by Tibet AS Array in five energy samples, 15, 50, 100, 300, and 1000 TeV, from top to bottom. Left panels show the solar time daily variations, with blue curves showing the first harmonic fit to the data and the black dashed curves indicating the expected CG effect due to the Earth's orbital motion around the sun, with an amplitude of 0.047% and an phase of 6 hr. Right panels show the antisidereal time daily variations and the first harmonic fitting results.